

Measurement of the atom-surface van der Waals interaction by transmission spectroscopy in a wedged nano-cell

T. Peyrot, N. Šibalić, Y.R.P. Sortais, and A. Browaeys
*Laboratoire Charles Fabry, Institut d'Optique Graduate School,
CNRS, Université Paris-Saclay, F-91127 Palaiseau Cedex, France*

A. Sargsyan and D. Sarkisyan
Institute for Physical Research, National Academy of Sciences - Ashtarak 2, 0203, Armenia

I.G. Hughes and C.S. Adams
Department of Physics, Rochester Building, Durham University, South Road, Durham DH1 3LE, United Kingdom
(Dated: January 14, 2022)

We demonstrate a method for measuring atom-surface interactions using transmission spectroscopy of thermal vapors confined in a wedged nano-cell. The wedged shape of the cell allows complementary measurements of both the bulk atomic vapor and atoms close to surfaces experiencing strong van der Waals atom-surface interaction. These are used to tightly constrain the dipole-dipole collisional parameters of a theoretical model for transmission spectra that accounts for atom-surface interactions, cavity effects, collisions with the surface of the cell and atomic motion. We illustrate this method on a cesium vapor in a sapphire cell, find $C_3 = 1.3 \pm 0.1 \text{ kHz} \cdot \mu\text{m}^3$ and demonstrate that even the weakest of the van der Waals atom-surface interaction coefficients — for ground-state alkali atom transitions — can be determined with a very good precision. This result paves the way towards a precise quantitative characterization of atom-surface interactions in a wide range of atom-based nano-devices.

Atoms close to surfaces offer new possibilities for engineered atom-atom and atom-light interactions through light confinement and surface mode excitations [1–4], ultimately down to the single-photon level [5–7]. This has stimulated a recent growth in the number of platforms where atoms are kept close to surfaces, ranging from nano-fibers [4, 8–11] and nano-cells [12, 13] to waveguides [14] and microtoroidal optical resonators [6]. Simultaneously, shrinking the dimensions of atom-based sensors [15–17] increases the number of atoms close to a surface relative to atoms in the bulk. Atom-surface interactions are therefore becoming increasingly important: they may limit the ultimate achievable precision of atom vapor sensors and they are crucial in understanding the dynamics in each new platform [6, 10, 11]. However, despite their significance, direct measurements of atom-surface interactions are scarce.

Measuring the van der Waals (vdW) atom-surface interaction — that scales with the distance z to the surface as $1/z^3$ [18] — is challenging as it requires placing the atoms in a given internal state at a distance $z < \lambda/(2\pi)$ from the surface [19]. Here λ is the wavelength of the strongest atomic transition from the considered state. Previous experiments on vdW atom-surface interactions used sophisticated techniques like reflections of cold atoms on a surface [20, 21], high-lying atomic states [22] or both [24]. High-lying states allow easier access to the vdW regime as: (i) transitions among higher-lying states correspond to longer wavelengths λ , relaxing the constrain on the atom-surface distance; and (ii) these transitions have larger dipole matrix elements, resulting in a stronger vdW coefficient C_3 in the atom-surface potential $V(z) = -C_3/z^3$. However, for many applications [2–6, 10–14], it is the properties

of the ground-state atom-surface potential that are of most interest.

Spectroscopy of thermal vapors contained in cells [22, 23, 25, 26] is an attractive method for the measurement of atom-surface interactions, since it can be used for a large range of vapors, atomic or molecular, and surfaces. However, measurements have low precision for weak vdW interaction strengths of ground state atoms, mainly limited by the uncertainty in estimating collisional processes in dense vapors [22, 25]. A recent method that measured the ground state vdW interaction based on *fluorescence* spectroscopy in low-density thermal vapors [27] raised debate [28] about the absolute achievable precision of the measurements, since the theoretical model used [27] neglected atomic motion in the spatially varying atom-surface potential. Finding simple and precise methods that would allow reliable extraction of the ground-state atom-surface potential parameters, and characterization of the atom dynamics in the proximity of surfaces in new platforms, remains an open goal.

Here, we demonstrate a new method for measuring the atom-surface interaction. Using a wedged nano-cell we obtain *transmission* spectra for a vapor thicknesses range of $L = 50 - 275 \text{ nm}$. This allows access both to the region where vdW interactions have strong effects on the total transmission signal, and the region where atoms in the bulk, not affected by the vdW induced shifts, dominantly contribute. Spectra from the thick region yield the collisional parameters for the bulk atomic vapor, thus allowing reliable fitting of thin-region spectra using our model. The model includes atomic motion in a spatially varying atom-surface potential, in addition to other surface-induced transient ef-

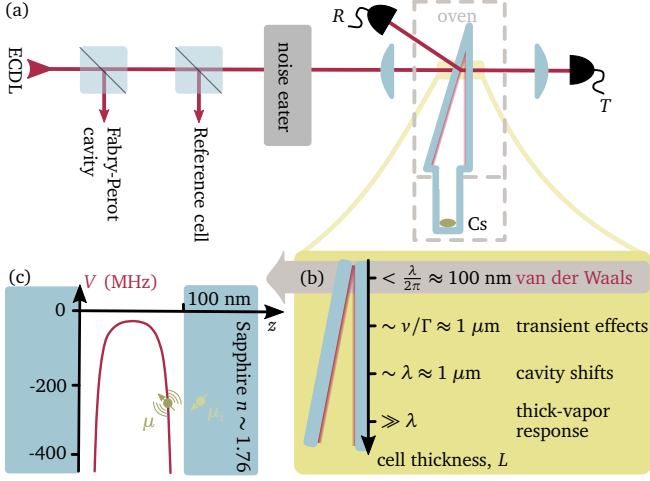


FIG. 1. (a) A frequency-calibrated, intensity-stabilized external cavity diode laser (ECDL) probes a cesium vapor confined in a wedged sapphire nano-cell. The cell thickness is locally measured using interference in the reflection signal R . (b) The wedged shape of the cell allows probing the transmission T in thick cell regions, where the contribution of atoms close to the surfaces is negligible compared to the contribution of the atoms in the bulk. It also allows going to sub-100 nm thick region where the atoms are strongly affected by the van der Waals potential, due to the interaction of their dipole with its image in the surface (c). This gives rise to a position z dependent level shift $V(z)$, here calculated for the D1 Cs transition.

fects [29]. This procedure allows measurement of the atom-surface potential even for the ground state transitions with a good precision. We illustrate it by a measurement of the vdW induced shift of the Cesium $6S_{1/2} \rightarrow 6P_{1/2}$ transition in the presence of a Sapphire surface. Our model significantly improves on a phenomenological one based on fitted line shift and broadening parameters, and shows excellent agreement with the measured spectra.

The experimental setup [29] is presented in Fig. 1(a). We use an external cavity diode laser (ECDL) to probe the D_1 ($\lambda = 894$ nm) transition of a cesium vapor contained in an ultra-thin wedged sapphire cell, with thickness varying from $L = 30$ nm to $2 \mu\text{m}$. We measure the *in-situ* vapor thickness L using interference resulting from the far off-resonant reflections from the wedge. With a beam waist of $50 \mu\text{m}$ ($1/e^2$ intensity), the uncertainty in the determination of L is 5 nm. The frequency scan of the ECDL is linearized using a Fabry-Perot cavity, and referenced to a standard 7 cm Cesium spectroscopic cell. The laser intensity is stabilized during the scan by an acousto-optic modulator-based noise eater. The wedged nano-cell is placed in a double oven: the bottom part containing the cesium reservoir is kept at 235°C , and sets the atom number density \mathcal{N} ; the top part with the wedged sapphire windows is kept at a temperature 30°C higher to avoid vapor condensation. The oven is temperature stabilised to $\sim 5^\circ\text{C}$. A low-noise photodiode is used to obtain the transmission signal T subtracted

from the background noise.

The theoretical analysis of transmission spectra in nano-cells is significantly more complicated than for transmission through bulk vapor [30]. With the reduction of the vapor thickness L , a number of effects starts to play a role [Fig. 1(b)]: (i) for micrometer thick layers, the cell walls act as a low-finesse cavity, resulting in level shifts [31]; (ii) the cell windows also cause dephasing of atoms upon direct collisions [32]. Atoms flying off the walls experience transient dynamics during a time $1/\Gamma$, with Γ the collisionally-broadened linewidth. For a cell thickness below v/Γ (v is the average atom velocity), a significant number of probed atoms experience the transient regime, which significantly modifies the measured transmission [29]. For cesium atoms at a temperature of $\sim 200^\circ\text{C}$ this corresponds to a distance of $\sim 1 \mu\text{m}$. Finally, (iii) at atom-surface distances $z < \lambda/(2\pi)$ atomic energy levels experience a vdW shift $V = -C_3/z^3$ [Fig. 1(c)]. This atom-surface interaction comes from the coupling between an atomic dipole and its image dipole in the sapphire surface [33]. To extract this vdW interaction at small atom-surface distances (iii), it is necessary to first account for the effects (i) and (ii) that modify the atom dynamics in thin cells even outside the range of the atom-surface potential.

We have recently developed a model for the atom response in the bulk [29], away from the influence of the vdW potential, following Refs. [34, 35]. To account for the transient atoms dynamics (ii) described above, we solve the optical Bloch equations [36] for the atom coherence field $\rho_{21}(z, v, \omega) = \rho_+(z, v, \omega)e^{ikz} + \rho_-(z, v, \omega)e^{-ikz}$, for each atomic velocity v class, where $k = 2\pi/\lambda = \omega/c$ is the laser field wave-vector *in vacuum*. Assuming a loss of coherence in atom-wall collisions [32], one obtains

$$\rho_{\pm}(z, v > 0) = i \frac{d_{FF'} E_{\pm}}{2\hbar v} \int_0^z \exp\left[\frac{\Lambda_{\pm}(z') - \Lambda_{\pm}(z)}{v}\right] dz', \quad (1)$$

$$\rho_{\pm}(z, v < 0) = -i \frac{d_{FF'} E_{\pm}}{2\hbar v} \int_z^L \exp\left[\frac{\Lambda_{\pm}(z') - \Lambda_{\pm}(z)}{v}\right] dz' \quad (2)$$

where E_{\pm} are the co- and counter-propagating driving fields along the z direction, and $d_{FF'}$ is the dipole moment for the hyperfine transition $F \rightarrow F'$. In a bulk cell, away from the range of the atom-surface potential, a level shift Δ_p and a broadening Γ_p of the transition arise due to the atom-atom collisional interaction. Thus, for $z > \lambda/(2\pi)$, Λ_{\pm} in Eqs. (1-2) is

$$\Lambda_{\pm}^{\text{bulk}}(z) = [(\Gamma_p + \Gamma_0)/2 - i(\Delta_{FF'} \mp kv)]z, \quad (3)$$

for a laser detuning $\Delta_{FF'} = \omega - \omega_{FF'} - \Delta_p$ from the transition at frequency $\omega_{FF'}$ with radiative linewidth $\Gamma_0/(2\pi) \approx 4.6$ MHz for the Cs D1 line [36]. Equations (1-2) can then be analytically solved, and the polarisation of the medium $P(z, \omega) = \sum_{F,F'} \int_{-\infty}^{\infty} dv 2\mathcal{N} M_b(v) d_{FF'} \rho(z, v, \omega)$ is obtained by summing the contributions from all velocity classes in the Maxwell-Boltzman distribution $M_b(v)$.

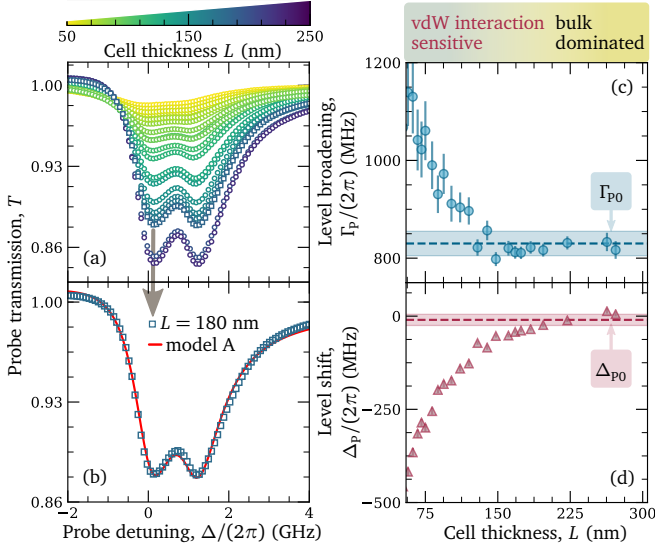


FIG. 2. Determination of the collisional broadening Γ_{p0} and shift Δ_{p0} in the bulk vapor. (a) Measured transmission spectra at 235 °C, for cell thickness L in range 50–225 nm. The left and right peaks correspond to the $F = 4 \rightarrow 3$ and $F = 4 \rightarrow 4$ transitions of the Cs D1 line respectively. Model A, not including atom-surface interactions, fits well spectra in the thick part of the cell (b), allowing the extraction of bulk properties of the vapor from values obtained for large L (c–d). For small L , the influence of the atom-surface interactions appears as an additional thickness-dependent line broadening and transition shift.

In order to include the cavity effects (i), we take into account the transmission $t_1 = 2n/(1+n)$ and reflection $r_2 = (1-n)/(1+n)$ coefficients of the driving field E_0 at the two sapphire cell walls (refractive index n). Assuming an optically dilute atomic medium, we neglect the contribution of atoms to the driving field E_{\pm} inside the cavity, so that $E_+ e^{ikz} + E_- e^{-ikz} \simeq t_1/[1 - r_2^2 \exp(2ikL)] E_0 \{ \exp[ikz] + r_2 \exp[ik(2L-z)] \}$. Similarly, the radiated atomic fields E_{A+} and E_{A-} initially co- or counter-propagating along the z -axis respectively [36], can be reflected multiple times inside the cavity [29]. They give rise to an atom induced field outside the cavity

$$E_{A\pm}(z) = \frac{t_2}{1 - r_2^2 e^{2ikL}} \frac{ik}{2\epsilon_0} \int_0^L dz' P(z', \omega) \exp[\pm ik(z-z')], \quad (4)$$

in the direction of initial emission, and fields $r_2 \exp[2ik(L-z)] E_{A+}$ and $r_2 \exp(2ikz) E_{A-}$ respectively in the opposite direction [36], where $t_2 = 2/(1+n)$. Finally, we obtain the transmission factor through the thin cell system $T = |E_T/E_{0+}|^2$, where $E_T = E_{0+} + E_{A+} + r_2 \exp(2ikz) E_{A-}$ is a superposition of the transmitted atom-induced field and transmitted driving field $E_{0+} = t_1 t_2/[1 - r_2^2 \exp(2ikL)] E_0 \exp(ikz)$.

The model described above (from now on Model A) fits well the measured transmission spectra [Fig. 2(a)] for cell thicknesses $L \geq 150$ nm [see for example Fig. 2(b)],

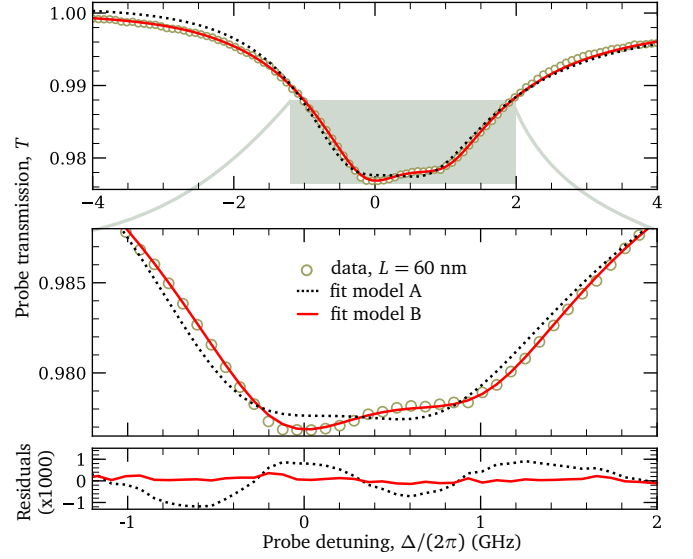


FIG. 3. Comparison of Model B that accounts for vdW interactions with phenomenological Model A. Model A (dotted line), not including atom-surface interactions, misses line-shape features for spectra in the thin cell region (circles), as highlighted on the zoomed inset. This is despite the fact that in addition to temperature, we take the broadening Γ_p and shift Δ_p as free parameters to phenomenologically account for atom-surface interactions. Model B (solid line) — that includes atom motion in the spatially dependent van der Waals potential explicitly — reproduces the asymmetric double-peak feature perfectly, with only the temperature and C_3 as free parameters when imposing bulk-determined line shift $\Delta_p = \Delta_{p0}$ and broadening $\Gamma_p = \Gamma_{p0}$.

where the signal is dominated by atoms far from the surface. In this region, fitting the temperature, level shift Δ_p and broadening Γ_p allows us to obtain the collisional self-broadening $\Gamma_{p0}/(2\pi) = 830 \pm 10$ MHz [Fig. 2(c)] and line shift $\Delta_{p0}/(2\pi) = -10 \pm 20$ MHz [Fig. 2(d)] in the bulk vapor, arising solely from atom-atom collisions. The value and error bar are the mean and standard error of the fitted values for cell thicknesses $L \geq 175$ nm. The measured broadening is in good agreement with theoretical predictions [37] at 235 °C.

For cell thicknesses $L \lesssim 150$ nm, the contribution from atoms close to the surface becomes significant. The vdW interaction [Fig. 1(c)] offsets the $6S_{1/2}$ and $6P_{1/2}$ levels by different amounts due to the different vdW C_3 coefficients for the two states. Model A captures this atom-surface interaction phenomenologically as a cell thickness dependent shift and broadening, as shown in Fig. 2(c-d). However, this phenomenological fit does not provide direct access to the C_3 vdW coefficient. In addition, Fig. 3 indicates that fine features of thin-cell spectra are not captured by Model A. This motivates extending the model to explicitly include the spatially varying vdW potential.

To do so, we now make the transition frequency spatially dependent: $\omega_{FF'} \rightarrow \omega_{FF'} - V(z)$. The atom-surface position dependent shift of the D1 transition frequency is $V(z) =$

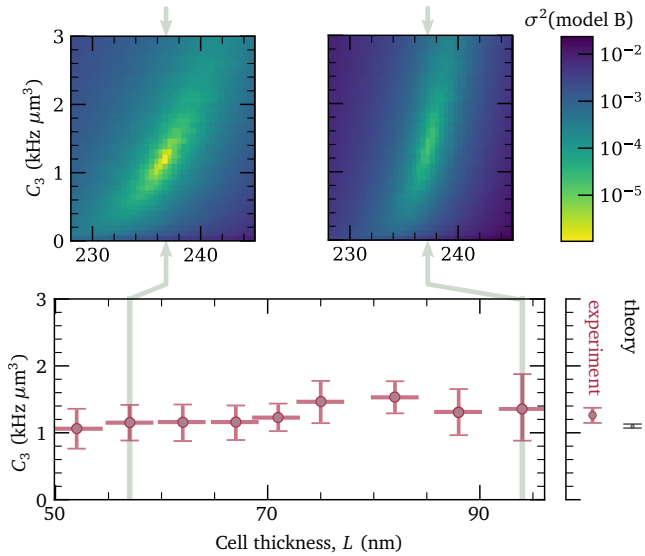


FIG. 4. Determination of the C_3 coefficient for the D1 line of Cs atoms close to the sapphire surface. Main plot: C_3 (circles) obtained by fitting Model B to the transmission spectra for different cell thickness. Error bars are systematic. Top insets: temperature- C_3 maps of the sum of squared residuals σ^2 for Model B, for two cell thicknesses indicated by vertical shaded bars on the main plot. The final value of C_3 , obtained as a weighted average, is in excellent agreement with the theoretical prediction (side scale).

$-C_3[1/z^3 + 1/(L-z)^3]$, where $C_3 = C_3[6P_{1/2}] - C_3[6S_{1/2}]$. In summing independently the potentials of each surface, we account only for the interaction of the atomic dipole with its image from the two surfaces. Image dipoles of image dipoles have contributions smaller than $\sim 3\%$ [36]. Solving the Bloch equations leads to the solution for the atomic coherence field of the same form as in Eqs. (1-2), except that now

$$\Lambda_{\pm}(z) = \left\{ \frac{\Gamma_0 + \Gamma_{p0}}{2} - i(\omega - \omega_{FF'} - \Delta_{p0} \mp kv) + iC_3 \left[\frac{1}{2z^3} - \frac{1}{2z(L-z)^2} \right] \right\} z. \quad (5)$$

Here we set the collisional broadening Γ_{p0} to be the same as in the bulk, which is justified as we are far from polaritonic resonances of the crystal surface [38]. The first part of Eq. (5) describes the bulk [Eq. (3)], while the second line is due to the atom-surface vdW potential. By using Eq (5) in Eq. (1-2), we include the *internal* atomic dynamics as the atoms move relative to the surface, thus experiencing *time-varying level shift* due to the vdW interaction $V(z)$, to obtain the coherence field for each velocity class at location z . In previous works based on fluorescence measurement [27], the motion was not accounted for [28]. For details of the numerical integration see Supplemental [36]. We call this Model B.

The result of the fitting of the data for a thin cell with $L = 60$ nm is shown in Fig. 3. Model B has only two free parameters, the temperature and C_3 , as Γ_{p0} and Δ_{p0} are

constrained to their bulk extracted values. Yet, it shows outstanding agreement compared to Model A that only phenomenologically accounts for atom-surface vdW interactions. In particular, the red-side asymmetry cannot be retrieved without taking properly the vdW shift into account. The value for C_3 is extracted from fitting the spectra for each cell thickness L (Fig. 4 main panel). Thin cells yield a larger fraction of atoms close to the surface, where the vdW potential induces large level shifts, and allow tighter constraints on the fitted parameters. This is visible on the map of the sum of squared residuals (Fig. 4 top insets), where the region that minimizes σ^2 is more tightly localized along the C_3 -axis for thin cells. The error bars on C_3 (main panel of Fig. 4) are systematic and result from propagating errors on the cell thickness and the fitted bulk vapor parameters Γ_{p0} and Δ_{p0} [36]. Assuming no dependence on L , the final value for C_3 is obtained as an average of the fitted values for different cell thicknesses weighted by their individual error bars [39]. We obtain $C_3 = 1.3 \pm 0.1 \text{ kHz} \cdot \mu\text{m}^3$, in good agreement (Fig. 4 side scale) with the theoretical value $C_3^{\text{th}} = 1.10 \pm 0.03 \text{ kHz} \cdot \mu\text{m}^3$ predicted from the Lifshitz theory of vdW interactions [36, 40], based on the refractive index of sapphire [41] and the latest calculations of dipole matrix elements for low-lying cesium transitions [42, 43].

In conclusion, we have demonstrated a method to measure the interaction between an atom and a surface. It relies on comparing the transmission of a laser beam through a wedged nano-cell filled with an atomic vapor to a theoretical model including the atom-surface interaction, cavity effects, collisions with surfaces of the cell and atomic motion. The wedged cell provides simultaneous access to the bulk vapor properties, tightly constraining theoretical parameters, and to thin cell regions with strong vdW interaction. We have illustrated the method with thermal cesium atoms confined within a sapphire cell and measured the D1 transition shift due to the cesium-sapphire interaction. Our model yields transmission predictions in excellent agreement with the experimental data. The measured C_3 coefficient is consistent with the non-resonant Lifshitz theory. Further improvements in precision are expected from adapting this work to fluorescence measurements, as better signal to noise ratio lead to a better determination of collisional properties as well as a reduction of statistical errors in extremely thin regions. Finally, this work opens the way to quantitative analysis of atom dynamics close to surfaces in new platforms [6, 10, 11], the search for predicted atom-surface repulsive potential [26] and bound-states [44], and the examination of short- [45] and long-range [46] limits of atom-surface potential, using thermal vapor spectroscopy. The data and the code for theoretical model are both available [47, 48].

We thank A. Laliotis and J. Keaveney for fruitful discussions. T. Peyrot is supported by the DGA-DSTL fellowship 2015600028. N. Š. is supported by EU Horizon 2020 (CO-QUDE, Marie Skłodowska-Curie fellowship No 786702). We also acknowledge financial support from EPSRC (grant

EP/R002061/1) and Durham University.

-
- [1] D. E. Chang, J. S. Douglas, A. González-Tudela, C. L. Hung, and H. J. Kimble, *Reviews of Modern Physics* **90**, 31002 (2018).
- [2] P. Lodahl, S. Mahmoodian, S. Stobbe, A. Rauschenbeutel, P. Schneeweiss, J. Volz, H. Pichler, and P. Zoller, *Nature* **541**, 473 (2017).
- [3] C. Stehle, C. Zimmermann, and S. Slama, *Nature Physics* **10**, 937 (2014).
- [4] R. Mitsch, C. Sayrin, B. Albrecht, P. Schneeweiss, and A. Rauschenbeutel, *Nature Communications* **5**, 5713 (2014).
- [5] D. Chang, A. Sørensen, E. Demler, and M. Lukin, *Nature Physics* **3**, 807 (2007).
- [6] T. Aoki, H. Lee, E. Ostby, D. J. Alton, H. J. Kimble, N. P. Stern, and K. J. Vahala, *Nature Physics* **7**, 159 (2010).
- [7] D. E. Chang, V. Vuletić, and M. D. Lukin, *Nature Photonics* **8**, 685 (2014).
- [8] F. L. Kien, V. I. Balykin, and K. Hakuta, *Physical Review A* **70**, 063403 (2004).
- [9] E. Vetsch, D. Reitz, G. Sagué, R. Schmidt, S. T. Dawkins, and A. Rauschenbeutel, *Physical Review Letters* **104**, 203603 (2010).
- [10] K. Deasy, C. F. Phelan, V. G. Truong, S. Nic Chormaic, and M. Daly, *New Journal of Physics* **16**, 053052 (2014).
- [11] B. D. Patterson, P. Solano, P. S. Julienne, L. A. Orozco, and S. L. Rolston, *Physical Review A* **97**, 032509 (2018).
- [12] D. Sarkisyan, D. Bloch, A. Papoyan, and M. Ducloy, *Optics Comm* **200**, 201 (2001).
- [13] T. Peyrot, C. Beurthe, S. Coumar, M. Roulliay, K. Perronet, P. Bonnay, C. S. Adams, A. Browaeys, and Y. R. P. Sortais, *Optics Letters* **44**, 1940 (2019).
- [14] R. Ritter, N. Gruhler, H. Dobbertin, H. Kübler, S. Scheel, W. Pernice, T. Pfau, and R. Löw, *Physical Review X* **8**, 021032 (2018).
- [15] S. Knappe, P. D. D. Schwindt, V. Shah, L. Hollberg, J. Kitching, L. Liew, and J. Moreland, *Optics Express* **13**, 1249 (2005).
- [16] R. T. Wakai, G. S. Smetana, T. G. Walker, M. Kauer, and R. Wyllie, *Physics in Medicine and Biology* **57**, 2619 (2012).
- [17] C. G. Wade, N. Šibalić, N. R. de Melo, J. M. Kondo, C. S. Adams, and K. J. Weatherill, *Nature Photonics* **11**, 40 (2017).
- [18] E. A. Hinds, in *Advances In Atomic, Molecular, and Optical Physics*, Vol. 28 (1991) p. 237.
- [19] At larger distances interaction potential retardation effects have to be taken into account, resulting in Casimir-Polder potential $\propto z^{-4}$. See e.g. the review [18].
- [20] A. Landragin, J. Y. Courtois, G. Labeyrie, N. Vansteenkiste, C. I. Westbrook, and A. Aspect, *Physical Review Letters* **77**, 1464 (1996).
- [21] A. K. Mohapatra and C. S. Unnikrishnan, *Europhysics Letters* **73**, 839 (2006).
- [22] M. Fichet, G. Dutier, A. Yarovitsky, P. Todorov, I. Hamdi, I. Maurin, S. Saltiel, D. Sarkisyan, M. P. Gorza, D. Bloch, and M. Ducloy, *EPL* **77**, 54001 (2007).
- [23] A. Sargsyan, A. Papoyan, I. G. Hughes, C. S. Adams, and D. Sarkisyan, Selective reflection from an Rb layer with a thickness below $\lambda/12$ and applications, *Opt.Lett* **8**, 42 (2017).
- [24] V. Sandoghdar, C. I. Sukenik, E. A. Hinds, and S. Haroche, *Physical Review Letters* **68**, 3432 (1992).
- [25] M. Oria, M. Chevrollier, D. Bloch, M. Fichet, and M. Ducloy, *Europhysics Letters* **14**, 527 (1991).
- [26] H. Failache, S. Saltiel, M. Fichet, D. Bloch, and M. Ducloy, *Physical Review Letters* **83**, 5467 (1999).
- [27] K. A. Whittaker, J. Keaveney, I. G. Hughes, A. Sargsyan, D. Sarkisyan, and C. S. Adams, *Physical Review Letters* **112**, 253201 (2014).
- [28] D. Bloch, *Physical Review Letters* **114**, 049301 (2015).
- [29] T. Peyrot, Y. R. P. Sortais, J. J. Greffet, A. Browaeys, A. Sargsyan, J. Keaveney, I. G. Hughes, and C. S. Adams, *Physical Review Letters* **122**, 113401 (2019).
- [30] M. A. Zentile, J. Keaveney, L. Weller, D. J. Whiting, C. S. Adams, and I. G. Hughes, *Computer Physics Communications* **189**, 162 (2015).
- [31] T. Peyrot, Y. R. P. Sortais, A. Browaeys, A. Sargsyan, D. Sarkisyan, J. Keaveney, I. G. Hughes, and C. S. Adams, *Physical Review Letters* **120**, 243401 (2018).
- [32] M. F. H. Schuurmans, *Le Journal de Physique* **37**, 469 (1976).
- [33] M. Fichet, F. Schuller, D. Bloch, and M. Ducloy, *Physical Review A* **51**, 1553 (1995).
- [34] D. Bloch and M. Ducloy, in *Advances in atomic, molecular, and optical physics*, Vol. 50, edited by B. Bederson and H. Walther (Academic Press, 2005) p. 91.
- [35] G. Dutier, S. Saltiel, D. Bloch, and M. Ducloy, *Journal of the Optical Society of America B* **20**, 793 (2003).
- [36] Authors, Supplemental material.
- [37] L. Weller, R. J. Bettles, P. Siddons, C. S. Adams, and I. G. Hughes, *Journal of Physics B: Atomic, Molecular and Optical Physics* **44**, 195006 (2011).
- [38] H. Failache, S. Saltiel, A. Fischer, D. Bloch, and M. Ducloy, *Physical Review Letters* **88**, 243603 (2002).
- [39] I. G. Hughes and T. P. A. Hase, *Measurements and their Uncertainties* (Oxford University Press, Oxford, 2010).
- [40] E. Lifshitz, *Soviet Physics JETP* **2**, 73 (1956).
- [41] M. J. Weber, ed., *Handbook of Optical Materials* (CRC Press, 2003).
- [42] M. S. Safronova, U. I. Safronova, and C. W. Clark, *Physical Review A* **94**, 012505 (2016).
- [43] N. Šibalić, J. D. Pritchard, C. S. Adams, and K. J. Weatherill, *Computer Physics Communications* **220**, 319 (2016).
- [44] E. G. Lima, M. Chevrollier, O. D. Lorenzo, P. C. Segundo, and M. Oria, *Physical Review A* **62**, 013410 (2000).
- [45] M. C. Vargas and W. L. Mochán, *Surface Science* **409**, 130 (1998).
- [46] J. C. A. Carvalho, P. Pedri, M. Ducloy, and A. Laliotis, *Physical Review A* **97**, 023806 (2018).
- [47] Data is available at [10.5281/zenodo.2653099](https://zenodo.org/record/2653099)
- [48] Code is available at <https://github.com/thermal-vapours/TAS-Transmission-Atom-Surface>

Supplemental Material: Measurement of the atom-surface van der Waals interaction by transmission spectroscopy in wedged nano-cell

T. Peyrot, N. Šibalić, Y.R.P. Sortais, and A. Browaeys
*Laboratoire Charles Fabry, Institut d'Optique Graduate School,
CNRS, Université Paris-Saclay, F-91127 Palaiseau Cedex, France*

A. Sargsyan and D. Sarkisyan
Institute for Physical Research, National Academy of Sciences - Ashtarak 2, 0203, Armenia

I.G. Hughes and C.S. Adams
Department of Physics, Rochester Building, Durham University, South Road, Durham DH1 3LE, United Kingdom
(Dated: January 14, 2022)

Here we detail the derivation of the theoretical model introduced in the main text, before discussing the error analysis and the theoretical predictions for the van der Waals (vdW) C_3 coefficient. In Sec. IA, we derive the atom coherence field inside the nano-cell, starting from the optical Bloch equations and including the vdW atom-surface interaction, the atomic motion, and the atom-surface collisions. Based on that result, we calculate in Sec. IB the optical field transmitted through a thin layer of atomic vapor, including optical cavity effects induced by the walls of the nano-cell. We present in Sec. II the procedure for estimating the error bars on the experimentally measured C_3 . Finally the theoretical calculation of C_3^{th} , and the numerical values of the dipole matrix elements used are presented in Sec. III.

I. DERIVATION OF THE VAPOR-CELL TRANSMISSION

In this Section, we derive the expression of the transmission through the atomic vapor slab, including the optical cavity effect due to the sapphire windows of the nano-cell and the vdW atom-surface interaction. We start by deriving the expression of the polarisation $P(z, \omega)$ of the ensemble of atoms and we subsequently compute the transmission through the nano-cell. The derivation is done in the limit of an optically thin vapor.

A. Calculation of the vapor polarisation P

We use a 1D model for the propagation along the z axis of the field through the vapor. We decompose the linearly polarized, monochromatic field driving the atom inside the cavity formed by the sapphire plates

$$E(z, t) = \frac{1}{2} [E(z)e^{-i\omega t} + E^*(z)e^{i\omega t}], \quad (1)$$

and the polarisation of the atomic vapor

$$P(z, t) = \frac{1}{2} [P(z)e^{-i\omega t} + P^*(z)e^{i\omega t}], \quad (2)$$

in their positive and negative frequency components. We first consider a given atomic transition between ground and excited states, with respective hyperfine states F and F' . The transition frequency is $\omega_{FF'}$, the total homogeneous linewidth

Γ_t , and the dipole matrix element $d_{FF'}$ for the driven transition by the linearly polarized laser field. For this transition, we introduce the classical coherence field $\rho_{21}(z, t, v) = \langle \rho_{21}^{(i)}(t, v) \rangle_{\text{atoms}}$ where $\langle \dots \rangle$ is the configuration average of the coherences $\rho_{21}^{(i)}$ of all atoms i located within the $(z, z + \delta z)$ slab and with velocities in the range $(v, v + \delta v)$ where $\delta z, \delta v \rightarrow 0$. The evolution of this field is given by the hydrodynamic equation:

$$\frac{\partial \rho_{21}(z, t, v)}{\partial t} = \underbrace{-i\omega_{FF'} \rho_{21}(z, t, v) + i \frac{d_{FF'} E(z, t)}{\hbar} - \frac{\Gamma_t}{2} \rho_{21}(z, t, v)}_{\text{Internal atom evolution (Bloch equations)}} \underbrace{-v \frac{\partial \rho_{21}(z, t, v)}{\partial z}}_{\text{atoms flying into and out from the slab at position } z}. \quad (3)$$

The first part of the right hand side of the equation is the standard Bloch equations for the evolution of the coherence under weak driving, when the population of the excited state can be neglected ($\rho_{22} \rightarrow 0$) [1]. In addition, since the field is defined as an average over many atoms at a given location z , it can also change due to atoms flying into and out of the vapor slab at position z . This is accounted for by the second part of the right-hand side of the Eq. (3), which appears owing to the fact that we consider the coherence *field* rather than the coherence of a given atom. It is valid assuming that the vapor is homogeneous, i.e. the atom number density \mathcal{N} for a given velocity is the same everywhere in the vapor [$\partial \mathcal{N}(z, v)/\partial z = 0$]. This is a very good approximation as long as the kinetic energy of the atoms is much larger than the potential energy induced by the vdW interactions, i.e. for $z > (2C_3/k_B T)^{1/3} = 0.6$ nm. Using Eq. (1) and the rotating wave approximation, we obtain the time-independent equation

$$v \frac{\partial \rho_{21}(z, v)}{\partial z} = - \left[\frac{\Gamma_t}{2} - i\Delta_{FF'} \right] \rho_{21}(z, v) + i \frac{d_{FF'} E(z)}{2\hbar}, \quad (4)$$

where $\Delta_{FF'} = \omega - \omega_{FF'}$ is the laser frequency detuning from the atomic transition. For the general driving field

$$E(z) = E_+ e^{ikz} + E_- e^{-ikz}, \quad (5)$$

consisting of the co-propagating E_+ and counter-propagating E_- field along the z axis with $k = \omega/c$ the laser wave-vector, we write the coherence as

$$\rho_{21}(z, v) = \rho_+(z, v) e^{ikz} + \rho_-(z, v) e^{-ikz}. \quad (6)$$

We thus obtain the following two equations from Eq. (4)

$$v \frac{\partial \rho_+}{\partial z} = - [\Gamma_t/2 - i(\Delta_{FF'} - kv)] \rho_+ + i \frac{d_{FF'} E_+}{2\hbar}, \quad (7)$$

$$v \frac{\partial \rho_-}{\partial z} = - [\Gamma_t/2 - i(\Delta_{FF'} + kv)] \rho_- + i \frac{d_{FF'} E_-}{2\hbar}. \quad (8)$$

In the two expressions above, both Γ_t and $\omega_{FF'}$ may depends on z , for example due to the atom-surface interaction potential. Using the variation of constant method for differential equations, we find for $v \neq 0$

$$\rho_+(z, v) = \rho_+(z_0, v) e^{-\Lambda_+/v} + i \frac{d_{FF'} E_+}{2\hbar v} \int_{z_0}^z dz' \exp \left[\frac{\Lambda_+(z') - \Lambda_+(z)}{v} \right], \quad (9)$$

$$\rho_-(z, v) = \rho_-(z_0, v) e^{-\Lambda_-/v} + i \frac{d_{FF'} E_-}{2\hbar v} \int_{z_0}^z dz' \exp \left[\frac{\Lambda_-(z') - \Lambda_-(z)}{v} \right], \quad (10)$$

where the primitive:

$$\Lambda_{\pm}(z) = \int^z \frac{\Gamma_t(u)}{2} - i[\Delta_{FF'}(u) \mp kv] du. \quad (11)$$

Assuming a loss of coherence resulting from the collisions of the atoms with the cell walls [2] (quenching collisions) leads to the boundary conditions $\rho_{\pm}(v > 0, z = 0) = \rho_{\pm}(v < 0, z = L) = 0$. Three cases can be distinguished:

(i) $\nu > 0$

$$\rho_+(z, \nu > 0) = i \frac{d_{FF'} E_+}{2\hbar\nu} \int_0^z dz' \exp\left[\frac{\Lambda_+(z') - \Lambda_+(z)}{\nu}\right], \quad (12)$$

$$\rho_-(z, \nu > 0) = i \frac{d_{FF'} E_-}{2\hbar\nu} \int_0^z dz' \exp\left[\frac{\Lambda_-(z') - \Lambda_-(z)}{\nu}\right]; \quad (13)$$

(ii) $\nu < 0$:

$$\rho_+(z, \nu < 0) = -i \frac{d_{FF'} E_+}{2\hbar\nu} \int_z^L dz' \exp\left[\frac{\Lambda_+(z') - \Lambda_+(z)}{\nu}\right], \quad (14)$$

$$\rho_-(z, \nu < 0) = -i \frac{d_{FF'} E_-}{2\hbar\nu} \int_z^L dz' \exp\left[\frac{\Lambda_-(z') - \Lambda_-(z)}{\nu}\right]; \quad (15)$$

$$(16)$$

(iii) $\nu = 0$:

$$\rho_{\pm}(z, \nu = 0) = \frac{id_{FF'} E_{\pm}/2\hbar}{\Gamma/2 - i\Delta_{FF'}}. \quad (17)$$

Now, knowing the coherences in Eq. (6), we calculate the polarisation given by Eq. (2) by integrating the total atomic dipole moment over the Maxwell-Boltzmann velocity distribution $M_b(\nu)$, and adding all relevant transitions $F \rightarrow F'$:

$$P(z, \omega) = \sum_{F, F'} \int_{-\infty}^{\infty} 2\mathcal{N} M_b(\nu) d_{FF'} [\rho_-(z, \nu, \omega) e^{-ikz} + \rho_+(z, \nu, \omega) e^{+ikz}] d\nu. \quad (18)$$

When the vdW potential is not taken into account, $\omega_{FF'}$ and Γ_i are independent of z . In this case, Eq. (18) gives analytical expressions that we derived in Ref. [3]. Here instead, we consider the atom-surface potential. As a consequence, a specific optical transition for an atom located at a distance z from the first surface is shifted as $\omega_{FF'}(z) = \omega_{FF'} - [C_3/z^3 + C_3/(L-z)^3]$. Far from any polaritonic resonances of the crystal surface, the linewidth may however be considered as independent of z and $\Gamma_{FF'} = \Gamma_0$ [4]. We can then calculate the integrals of Eq.(11):

$$\Lambda_{\pm} = \left\{ \frac{\Gamma}{2} - i \left[\Delta \mp kv - \frac{C_3}{2z^3} + \frac{C_3}{2z(L-z)^2} \right] \right\} z. \quad (19)$$

The expression now diverges for $z = 0$ and $z = L$. Besides none of equations (12), (13), (15) and (18) provide analytical solutions. These integrals are regularised by introducing a minimal cutoff distance $L_{\text{cut}} = 0.1$ nm from both surfaces. We have checked that it does not influence the results of the numerical computation.

B. Calculation of the driving and transmitted fields in the presence of the cavity

The cell walls present two interfaces for the incoming driving light E_0 (Fig. 1). First from the sapphire into the vacuum filled with the atomic vapor, with amplitude transmission $t_1 = 2n/(1+n)$ and reflection $r_1 = (n-1)/(1+n)$ coefficients given by the sapphire refractive index n . This is followed by the vapor-sapphire interface, with respective amplitude transmission $t_2 = 2/(1+n)$ and reflection $r_2 = (1-n)/(1+n)$ coefficients. In fact, multiple reflections of the driving field between the two

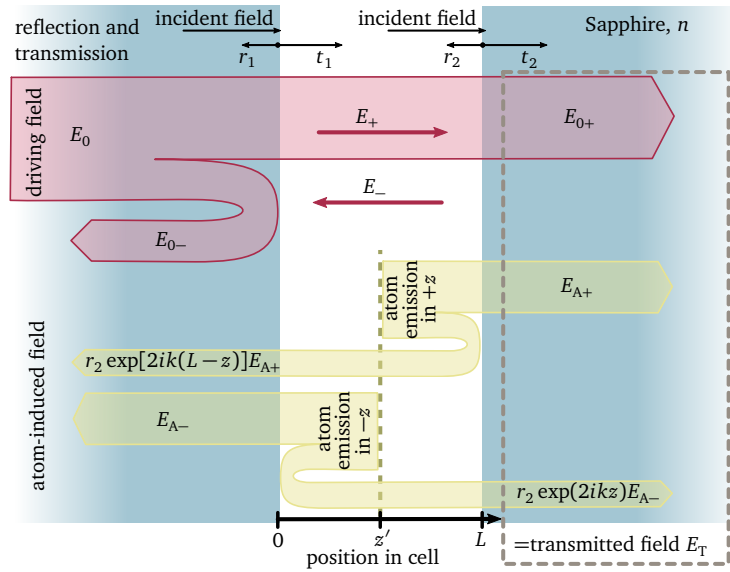


FIG. 1. Reflection and transmission of fields on sapphire-vapor and vapor-sapphire interfaces. Incident driving field E_0 is split by this interface into a transmitted field E_{0+} and a reflected field E_{0-} . Inside the low-finesse cavity formed by these two interfaces, the driving field gives rise to a field E_+ propagating along the z -axis direction, and a counter-propagating field E_- . The field emitted by the atoms *inside the cavity* in the forward direction after multiple reflections by the cavity results in the fields E_{A+} and $r_2 \exp[2ik(L-z)]E_{A+}$ propagating *outside the cavity* in the $+z$ and $-z$ directions respectively. Similarly, the field emitted initially by the atoms in $-z$ direction results in the fields E_{A-} and $r_2 \exp(2ikz)E_{A-}$ propagating *outside the cavity* in the $-z$ and $+z$ directions respectively.

nearly-parallel sapphire surfaces that form a low finesse cavity result in a total driving field *inside the cavity*, co-propagating along the z -axis direction:

$$E_+ = E_0 \frac{t_1}{1 - r_2^2 e^{2ikL}}, \quad (20)$$

and a counter-propagating driving field

$$E_- = E_0 \frac{t_1 r_2 e^{2ikL}}{1 - r_2^2 e^{2ikL}}. \quad (21)$$

Here $k = \omega/c$ is the field wave-vector *in vacuum*, as we assume that the vapor is optically thin so as to neglect its index of refraction. The driving field *after* the cavity is therefore

$$E_{0+} = E_0 \frac{t_1 t_2}{1 - r_2^2 e^{2ikL}}. \quad (22)$$

We now account for the field scattered by the polarisation of the atomic vapor. The field emitted by the atoms *inside the cavity* along the z axis ($+z$ direction), experiences multiple reflections between the two sapphire windows (see Fig. 1), resulting in the fields E_{A+} and $r_2 \exp[2ik(L-z)]E_{A+}$ propagating *outside the cavity* in the $+z$ and $-z$ direction respectively, where

$$E_{A+} = \frac{t_2}{1 - r_2^2 e^{2ikL}} \frac{ik}{2\epsilon_0} \int_0^L dz' P(z', \omega) e^{ik(z-z')}. \quad (23)$$

Similarly the field originally emitted by the atoms *inside the cavity* in $-z$ direction, after multiple reflections by the cell

windows results in fields E_{A-} and $r_2 \exp(2ikz)E_{A-}$ propagating *outside the cavity* in $-z$ and $+z$ directions, where

$$E_{A-} = \frac{t_2}{1 - r_2^2 e^{2ikL}} \frac{ik}{2\epsilon_0} \int_0^L dz' P(z', \omega) e^{-ik(z-z')}. \quad (24)$$

The transmitted field along the z -axis is then given by the sum of the driving field and atom-induced field contributions

$$E_{T+} = E_{0+} + E_{A+} + r_2 \exp(2ikz)E_{A-}. \quad (25)$$

The relative transmission is thus $T = |E_T/E_{0+}|^2$.

NOTE. We highlight one nano-cell peculiarity in comparison to more standard, thick cells, regarding directionality of emitted light. Using expression for polarisation Eq. (18) in Eq. (23) for emission along the laser beam, we obtain

$$E_{A+} \propto \int_0^L \rho_+ dz' + \int_0^L \rho_- e^{-2ikz'} dz'. \quad (26)$$

For thick cells ($L \gg \lambda$) and slowly varying coherence fields ρ_+ and ρ_- , we note that rapid integrand sign change in the second term prevents contribution of ρ_- to E_{A+} . We obtain that emission in the $z+$ direction is then dominated by the ρ_+ part of the coherence field. However for nano-cells $L \ll \lambda$, exponential factor is practically constant over the length of the cell, and we see that ρ_- *also contributes to the emission in the $z+$ direction*. This is expected if one keeps in mind that large atomic ensembles can emit light in a given direction thanks to the interference [given by Eq. (23)] from phase grating (c.f. Bragg grating) imprinted by the driving laser beam into the spatial variation of coherence phase. However, cells $L \ll \lambda$ are not thick enough to contain a single period λ of this phase variation (Bragg grating), and emission integration in Eq. (23) will not single out contribution of ρ_+ to polarisation [Eq. (18)]. Instead ρ_- will contribute to emission in forward direction too. In particular, note that this is not the consequence of reflection of the light emitted along $z-$ on the interface. Indeed the effect would exist even in the absence of cavity induced reflections. This effect can also be seen as a consequence of constrain on space-bandwidth product of Fourier transform in space, that for small total distances cannot distinguish between $+k$ and $-k$ components (c.f. Heisenberg relations), giving reduction of phase matching constrain for thin cells.

II. ESTIMATION OF THE ERROR BARS ON THE EXTRACTED C_3 VALUE

In this section, we explain how we have assigned the error bars for the C_3 coefficients extracted from the transmission spectra corresponding to various thicknesses presented in Fig.(4) of the main text. We subsequently derive the final value and uncertainty for the atom-surface coefficient.

To extract the transmission in intensity from the raw data, we need to divide the measured transmitted intensity by the intensity far from the atomic resonance. In normalizing the data, an issue arises due to a residual variation of the intensity not corrected by the stabilisation of the laser power during the scan across the atomic resonances. This residual variation may distort the lineshape and introduce unphysical shifts. Our normalization procedures therefore accounts for this nearly linear intensity variation. We have checked that a small variation of the residual slope of the intensity variation does not influence significantly the fitted C_3 value (on the order of few percent). We then checked that the statistical repetition of the measurements does not modify the extracted C_3 value.

As explained in the main text, in order to extra the C_3 coefficient, we fix the thickness measured with an uncertainty of 5 nm. Collisional linewidth and shift are also fixed to their bulk values Δ_{p0} and Γ_{p0} measured at large cell thicknesses.

These values are the average of the shifts Δ_p and broadenings Γ_p obtained for thicknesses $L \geq 175\text{nm}$, and the error bar on these parameters is the standard deviation of this ensemble of values. In order to assign an error bar to the C_3 coefficient, we perform an error propagation in the following way: we vary within their error intervals Δ_p and Γ_p and L and repeat the fitting procedure to find the C_3 that minimizes the sum of squared residuals. We thus obtain the systematic error on C_3 associated to the uncertainty in the determination of Δ_{p0} and Γ_{p0} . For each cell thickness L we then assign an error bar that encompasses all the C_3 values obtained in this way.

When applying this procedure, we find that the extracted C_3 is insensitive to the value of Γ_{p0} . On the contrary, it is very sensitive to the value of Δ_{p0} and L , which are by far the main contributors to the uncertainty of C_3 . The error bars assigned for each thickness in Fig. 4 of the main text correspond to the variation of C_3 by changing Δ_{p0} within ± 20 MHz range and L within ± 2.5 nm. For each thickness, the error bar associated to C_3 is the quadratic sum of the error due to Δ_{p0} and L .

In order to give a final value for the extracted C_3 , we make the final assumption that it does not vary with the cell thickness. This approximation supposes that retardation effects would not lead to an effective dependence of C_3 with L . The final value of the cesium-sapphire C_3 coefficient is then assigned, together with its error bar, as an average weighted by the individual points of the error-bars. We find:

$$C_3 = 1.3 \pm 0.1 \text{ kHz} \cdot \mu\text{m}^3 \quad (27)$$

III. THEORETICAL CALCULATION OF C_3^{th}

The level shift $V_a(z)$ experienced by an atom in a state $|a\rangle$, placed in front of a dielectric surface with refractive index $n(\omega)$ is given by (see for example [5]):

$$V_a(z) = -\frac{1}{4\pi\epsilon_0} \sum_{\text{states } |b\rangle} \frac{n(\omega_{ab})^2 - 1}{n(\omega_{ab})^2 + 1} \frac{|\mu_x^{\text{ab}}|^2 + |\mu_y^{\text{ab}}|^2 + 2|\mu_z^{\text{ab}}|^2}{16z^3} \equiv -\frac{C_3^a}{z^3}. \quad (28)$$

The prefactor depending on the refractive index $n(\omega_{ab})$ at the frequency ω_{ab} of an atomic transition $|a\rangle \rightarrow |b\rangle$ accounts for the strength of the image dipole formed inside the dielectric. It would be equal to 1 for a perfectly reflective surface. The sum is over all states $|b\rangle$ that are dipole-coupled to $|a\rangle$, and $\mu_{x\dots z}^{\text{ab}}$ are the dipole matrix elements corresponding to the dipole orientations along the x , y and z axis respectively. Knowing the refractive index of the surface for a range of frequencies and the dipole matrix elements of the corresponding transitions allows one to calculate the energy shift of a given state due to van der Waals interaction, as given in Table I. In this table, the dipole matrix elements are theoretically calculated values from Ref.[6] and Alkali Rydberg Calculator (ARC) Python package [7]. The refractive index of ordinary Sapphire is calculated from the data in Ref. [8]. Using the values in Table I, we finally obtain the theoretical van der Waals coefficient for the shift of the $6S_{1/2} \rightarrow 6P_{1/2}$ transition:

$$C_3^{\text{th}} = C_3[6P_{1/2}] - C_3[6S_{1/2}] = 1.10 \pm 0.03 \text{ kHz} \cdot \mu\text{m}^3. \quad (29)$$

The expression (28) used for $V_a(z)$ accounts only for the interaction of a dipole with its image in the sapphire. The interaction of dipole image with its dipole image, and higher, is neglected. The full potential would have the form [9]:

$$V_a^{\text{tot}}(z) = -\frac{1}{4\pi\epsilon_0} \sum_{\text{states } |b\rangle} \left\{ \frac{|\mu_x^{\text{ab}}|^2 + |\mu_y^{\text{ab}}|^2 + 2|\mu_z^{\text{ab}}|^2}{16} \sum_{m=0}^{\infty} \left[\frac{1}{(z+mL)^3} + \frac{1}{(L-z+mL)^3} \right] \delta(\omega_{ab})^{2m+1} \right. \\ \left. - \frac{|\mu_x^{\text{ab}}|^2 + |\mu_y^{\text{ab}}|^2 - 2|\mu_z^{\text{ab}}|^2}{16} \sum_{m=1}^{\infty} \frac{2}{(mL)^3} \delta(\omega_{ab})^{2m} \right\}, \quad (30)$$

where $\delta(\omega_{ab}) = [n(\omega_{ab})^2 - 1]/[n(\omega_{ab})^2 + 1]$ is a factor depending on the material, and where the first and second line correspond respectively to odd and even reflections. Due to spherical symmetry $|\mu_x|^2 = |\mu_y|^2 = |\mu_z|^2$ and the second term is zero. For the atoms in the middle of the cell, $z = L/2$ and the contribution of the $m = 1$ term will already be $1/3^3$ smaller (closer to the surfaces, the suppression will be even stronger) due to the larger distance between the atom and their image. The extra factor $\delta^2 \approx (0.5)^2$ leads to further suppression, giving a total contribution on the order of $\sim 1\%$ compared to the $m = 0$ term taken into account in the potential $V(z)$ used in the main text. Higher order reflections are even more suppressed. Thus the potential $V(z)$ used in the main text is a good approximation of the V^{tot} to within $\sim 3\%$.

TABLE I. Dominant contributions to the cesium-sapphire van der Waals constant C_3 for $6S_{1/2}$ and $6P_{1/2}$ states, with listed sources for dipole matrix elements μ^{ab} .

Hyperfine transition	contribution to C_3^a (kHz. μm^3)	Source
$6S_{1/2} \leftrightarrow 6P_{1/2}$	0.42	[6]
$6S_{1/2} \leftrightarrow 6P_{1/2}$	0.83	[6]
$6S_{1/2} \leftrightarrow 7P_{3/2}$	0.01	[6]
Total $C_3^{6S_{1/2}} =$		1.258(2)
$6P_{1/2} \leftrightarrow 6S_{1/2}$	0.42	[6]
$6P_{1/2} \leftrightarrow 7S_{1/2}$	0.37	[6]
$6P_{1/2} \leftrightarrow 8S_{1/2}$	0.02	[7]
$6P_{1/2} \leftrightarrow 5D_{3/2}$	1.01	[6]
$6P_{1/2} \leftrightarrow 6D_{3/2}$	0.37	[6]
$6P_{1/2} \leftrightarrow 7D_{3/2}$	0.09	[6]
$6P_{1/2} \leftrightarrow 8D_{3/2}$	0.04	[7]
$6P_{1/2} \leftrightarrow 9D_{3/2}$	0.02	[7]
$6P_{1/2} \leftrightarrow 10D_{3/2}$	0.01	[7]
Total $C_3^{6P_{1/2}} =$		2.36(3)

- [1] G. Grynberg, A. Aspect, and C. Fabre, *Introduction to Quantum Optics: From the Semi-classical Approach to Quantized Light* (Cambridge University Press, Cambridge, 2010).
- [2] M. F. H. Schuurmans, *Le Journal de Physique* **37**, 469 (1976).
- [3] T. Peyrot, Y. R. P. Sortais, J. J. Greffet, A. Browaeys, A. Sargsyan, J. Keaveney, I. G. Hughes, and C. S. Adams, *Physical Review Letters* **122**, 113401 (2019).
- [4] H. Failache, S. Saliel, A. Fischer, D. Bloch, and M. Ducloy, *Physical Review Letters* **88**, 243603 (2002).
- [5] M. Fichet, F. Schuller, D. Bloch, and M. Ducloy, *Physical Review A* **51**, 1553 (1995).
- [6] M. S. Safronova, U. I. Safronova, and C. W. Clark, *Physical Review A* **94**, 012505 (2016).
- [7] N. Šibalić, J. D. Pritchard, C. S. Adams, and K. J. Weatherill, *Computer Physics Communications* **220**, 319 (2016).
- [8] M. J. Weber, ed., *Handbook of Optical Materials* (CRC Press, 2003).
- [9] E. A. Hinds, in *Advances In Atomic, Molecular, and Optical Physics*, Vol. 28 (1991) p. 237.